Heterogeneous Multidimensional Data Deblurring

Ferréol Soulez, Éric Thiébaut, Alain Gressard, Raphaël Dauphin, Sébastien Bongard

HETEROGENEOUS MULTIDIMENSIONAL DATA DEBLURRING

Ferréol Soulez[1,2], *Éric Thiébaut*[1], *Alain Gressard*[3], *Raphaël Dauphin*[3], *Sbastien Bongard*[4]

[1]Centre de Recherche Astrophysique de Lyon, CNRS-UMR 5574, Université Lyon 1, Ecole Normale Supérieure de Lyon Observatoire de Lyon, 9 avenue Charles André, Saint-Genis Laval cedex, F-69561, France.

[2] Laboratoire Hubert Curien (ex-LTSI), CNRS-UMR 5516, Université Jean Monnet, 18 rue Pr Benoît Lauras, F-42000 Saint-Etienne, France.

[3] Service de Cardiologie de l'hôpital de la Croix Rousse, Hospices Civils de Lyon, France

[4] Lawrence Berkeley National Laboratory, CA, USA

ABSTRACT

We present a new scheme for deconvolution of heterogeneous multidimensional data (*e.g.* spatio-temporal or spatio-spectral). It is derived, in a very general way, following an inverse problem approach. This method exploits the continuity of both object and PSF along the different dimensions to elaborate separable constraints. This improves the effectiveness and the robustness of the deconvolution technique. We demonstrate these improvements by processing real X-ray video sequences (x,y,t) and astronomical multi-spectral images (x,y,λ).

1. INTRODUCTION

Nowadays, blind image deconvolution receives increasing attention from the academic world (see [1] for a review). Most of these works focus on image deconvolution and to our knowledge, excepted in the specific super-resolution field([2]), few of them ([3, 4, 5]) address the problem of deconvolving multidimensional data (*e.g.* series of images of a varying scene taken at different times or wavelengths). In this paper, we propose an algorithm for blind or conventionnal deconvolution of such multidimensional data. It uses correlation along every dimension to elaborate constraints and then perform effective deblurring. First we describe the model of image formation, then we talk about the likelihood and the different separable regularizations used in our approach. After a quick summary of the algorithm, we show two results in two different application fields: (i) a blind deconvolution of medical X-ray video sequences (x,y,t); (ii) a deconvolution of astronomical multi-spectral images (x,y,λ).

2. MODEL DESCRIPTION

In this paper we consider a multidimensional object $f(\boldsymbol{s})$ with heterogeneous dimensions $\boldsymbol{s} = (\boldsymbol{r}, t, \lambda)$ with $\boldsymbol{r} = (x,y)$ the spatial position, t the time and λ the wavelength. The data $g(\boldsymbol{s})$ are given by:

$$g(\boldsymbol{s}) = \int h(\boldsymbol{s}|\boldsymbol{s}')f(\boldsymbol{s}')d\boldsymbol{s}' + n(\boldsymbol{s}), \tag{1}$$

where $f(\boldsymbol{s}')$ is the object brightness distribution, $h(\boldsymbol{s}|\boldsymbol{s}')$ is the point spread function (PSF), and $n(\boldsymbol{s})$ accounts for the noise (source and detector). The PSF $h(\boldsymbol{s}|\boldsymbol{s}')$ is the observed brightness distribution at $\boldsymbol{s}$ for a point source located at $\boldsymbol{s}'$.

For data sampled on a rectangular grid of N pixels, T time frames and L wavelength channels, Eq. (1) can be written in a matrix form:

$$\boldsymbol{g} = \mathbf{H}\cdot\boldsymbol{f} + \boldsymbol{n}, \tag{2}$$

where $\boldsymbol{g}$ and $\boldsymbol{f}$ are stacked vectors of size $N\cdot T\cdot L$, $\boldsymbol{n}$ is a $N\cdot T\cdot L$ random vector and $\mathbf{H}$ is a $(N\cdot T\cdot L)\times(N\cdot T\cdot L)$ matrix. In other words:

$$g_{r,\lambda,t} = \sum_{r',t',\lambda'} H_{r,t,\lambda;r',\lambda',t'}\cdot f_{r',t',\lambda'} + n_{r,\lambda,t}\,. \tag{3}$$

If there is no spread between time frames or wavelength channels or both (*e.g.* $g_{r,\lambda,t} = \sum_{r'} H_{r',t,\lambda;r,\lambda,t}\cdot f_{r',t,\lambda} + n_{r,\lambda,t}$), $\mathbf{H}$ becomes block diagonal. In addition, if the PSF is shift invariant (isoplanatic), then Eq. (1) can be expressed using $*$ to denote spatial convolution and the first spatial row of $\mathbf{H}$ $\boldsymbol{h}_{t,\lambda} = [h_{r,t,\lambda}; \forall r]$:

$$\boldsymbol{g}_{t,\lambda} = \boldsymbol{h}_{t,\lambda} \underset{(r)}{*} \boldsymbol{f}_{t,\lambda} + \boldsymbol{n}_{t,\lambda}. \tag{4}$$

Under circulant approximation, this can be evaluated rapidly using FFT's.

3. INVERSE PROBLEM APPROACH

In blind deconvolution the object vector $\boldsymbol{f}$ and the PSF $\boldsymbol{h}$, both of size $N\cdot T\cdot L$, must be estimated from only $N\cdot T\cdot L$ measurements stacked in $\boldsymbol{g}$. This is a typical inverse problem, that can be solved in a penalized likelyhood or maximum a posteriori (MAP) framework [6].

This is achieved by estimating the couple $\{\boldsymbol{f}^+, \boldsymbol{h}^+\}$ that minimizes the cost function $\varepsilon(\boldsymbol{f},\boldsymbol{h})$:

$$\{\boldsymbol{f}^+, \boldsymbol{h}^+\} = \underset{\{\boldsymbol{f},\boldsymbol{h}\}}{\arg\min}\, \varepsilon(\boldsymbol{f},\boldsymbol{h}), \tag{5}$$

$$\varepsilon(\boldsymbol{f},\boldsymbol{h}) = \Phi_{\mathrm{lkl}}(\boldsymbol{f},\boldsymbol{h},\boldsymbol{g}) + \Phi_{\mathrm{obj}}(\boldsymbol{f}) + \Phi_{\mathrm{psf}}(\boldsymbol{h}), \tag{6}$$

This cost function $\varepsilon(\boldsymbol{f},\boldsymbol{h})$ is the sum of three terms: a *likelihood penalty* $\Phi_{\mathrm{lkl}}(\boldsymbol{f},\boldsymbol{h};\boldsymbol{g})$ ensuring the agreement between the model $\boldsymbol{f}*\boldsymbol{h}$ and the data $\boldsymbol{g}$, and two *regularization penalties* $\Phi_{\mathrm{obj}}(\boldsymbol{f})$ and $\Phi_{\mathrm{psf}}(\boldsymbol{h})$ introducing subjective *a priori* knowledge about the object and the PSF respectively.

In the case where the PSF is known (simple deconvolution), only the object vector $\boldsymbol{f}$ must be estimated. The criterion becomes:

$$\varepsilon(\boldsymbol{f}) = \Phi_{\mathrm{lkl}}(\boldsymbol{f},\boldsymbol{h},\boldsymbol{g}) + \Phi_{\mathrm{obj}}(\boldsymbol{f}). \tag{7}$$

3.1 The likelihood penalty term

For Gaussian noise, the likelihood penalty reads:

$$\Phi_{\text{lkl}}(\boldsymbol{f},\boldsymbol{h},\boldsymbol{g}) = [\boldsymbol{g}-\boldsymbol{m}(\boldsymbol{f},\boldsymbol{h})]^{\mathrm{T}}\cdot\mathbf{W}\cdot[\boldsymbol{g}-\boldsymbol{m}(\boldsymbol{f},\boldsymbol{h})], \quad (8)$$

where $\boldsymbol{m}(\boldsymbol{f},\boldsymbol{h})$ is the model and $\mathbf{W}$ is a weighting matrix accounting for the different noises (observation noise, detector noise, model errors...) and is the inverse of its covariance matrix: $\mathbf{W} = \mathbf{C}_{\text{noise}}^{-1}$. Using Eq. (2) the model is defined as:

$$\boldsymbol{m}(\boldsymbol{f},\boldsymbol{h}) = \mathbf{H}\cdot\boldsymbol{f}, \quad (9)$$

and can be evaluated using Eq. (4) for every (t,λ). If the noise is uncorrelated, the weighting matrix is diagonal $\mathbf{W} = \text{diag}(\boldsymbol{w})$ and Eq. (8) simplifies to:

$$\Phi_{\text{lkl}}(\boldsymbol{f},\boldsymbol{h},\boldsymbol{g}) = \sum_{r,t,\lambda} w_{r,t,\lambda}\left(\left(\mathbf{H}_{t,\lambda}\cdot\boldsymbol{f}_{t,\lambda}\right)_r - g_{r,t,\lambda}\right)^2, \quad (10)$$

where $1/w_{r,t,\lambda}$ is the noise variance for pixel r of frame t and channel λ. This model can cope with non-stationary noise and can be used to express confidence on measurements on each pixel of the data. Since unmeasured data have infinite variance, we can readily deal with missing (outside the field of view) or bad pixels as follows:

$$w_{r,t,\lambda} \overset{\text{def}}{=} \begin{cases} \text{Var}(g_{r,t,\lambda})^{-1} & \text{if } g_{r,t,\lambda} \text{ is measured,} \\ 0 & \text{otherwise.} \end{cases} \quad (11)$$

Except for very low detector noise (< few e^- per pixel), we can approximate the total noise (Gaussian detector noise plus Poissonnian signal noise) by a non stationary Gaussian noise:

$$w_{r,t,\lambda} \overset{\text{def}}{=} \begin{cases} \left(\gamma\max(g_{r,t,\lambda},0) + \sigma^2_{r,t,\lambda}\right)^{-1} & \text{if } g_{r,t,\lambda} \text{ is measured,} \\ 0 & \text{otherwise,} \end{cases} \quad (12)$$

where γ accounts for the quantization factor of the detector and $\sigma^2_{r,t,\lambda}$ is the variance of other approximately Gaussian noise (for example read-out noise) on the pixel (r,t,λ).

3.2 Separable *a priori*

As the different dimensions of the object are not homogeneous, we consider a separable regularization term for the object:

$$\Phi_{\text{obj}}(\boldsymbol{f}) = \Theta_{\text{obj}}(\boldsymbol{f}) + \Psi_{\text{obj}}(\boldsymbol{f}) + \Xi_{\text{obj}}(\boldsymbol{f}), \quad (13)$$

where $\Psi_{\text{obj}}(\boldsymbol{f})$ is a temporal regularization, $\Theta_{\text{obj}}(\boldsymbol{f})$ is a spatial regularization and $\Xi_{\text{obj}}(\boldsymbol{f})$ is the spectral regularization.

In the same way, we define a separable regularization for the PSF:

$$\Phi_{\text{psf}}(\boldsymbol{h}) = \Theta_{\text{psf}}(\boldsymbol{h}) + \Psi_{\text{psf}}(\boldsymbol{h}) + \Xi_{\text{psf}}(\boldsymbol{h}). \quad (14)$$

In order to be as general as possible, we use:

$$\Psi(\boldsymbol{x};\boldsymbol{\alpha}) = \sum_{r,\lambda}\alpha_{r,\lambda}\Omega_\Psi(\boldsymbol{x};r,\lambda), \quad (15)$$

$$\Theta(\boldsymbol{x};\boldsymbol{\beta}) = \sum_{t,\lambda}\beta_{t,\lambda}\Omega_\Theta(\boldsymbol{x};t,\lambda), \quad (16)$$

$$\Xi(\boldsymbol{x};\boldsymbol{\mu}) = \sum_{r,t}\mu_{r,t}\Omega_\Xi(\boldsymbol{x};r,t), \quad (17)$$

where $\boldsymbol{x} = \boldsymbol{f}$ or $\boldsymbol{h}$ and where the Ω's are metric functions. For instance, in Eq. (16), $\Omega_\Theta(\boldsymbol{x};t,\lambda)$ is the spatial regularization for a slice of $\boldsymbol{x}$ taken at given (t,λ) and $\beta_{t,\lambda}$ is the corresponding weight. The weights $\boldsymbol{\alpha}$, $\boldsymbol{\beta}$, and $\boldsymbol{\mu}$ are so-called hyper-parameters that have to be properly tuned. In what follows, we discuss the choice of the metric functions and of the hyper-parameters.

3.3 Regularizations functions

In image reconstruction many different kind of regularisation have been considered. In this section, we describe the particular functions that will be used in our tests.

3.3.1 Quadratic smoothness regularization

As noise mostly contaminates high frequencies, smoothness is the most effective regularization constraint to avoid amplification noise. The regularization function is then defined by:

$$\Omega_{\text{smooth}}(\boldsymbol{x};t,\lambda) = \left\|\mathbf{D}\cdot\boldsymbol{x}_{t,\lambda}\right\|_2^2, \quad (18)$$

where $\mathbf{D}$ is a finite difference operator along one or several homogeneous dimensions. This regularization is often used for spatial regularization. Using 1st order finite difference, Eq. (16) can be rewritten as:

$$\Theta_{\text{obj}}(\boldsymbol{x};\boldsymbol{\beta_{\text{obj}}}) = \sum_{t,\lambda}\beta^{\text{obj}}_{t,\lambda}\sum_r\sum_{r'\in V_r}\left\|\frac{x_{r,t,\lambda}-x_{r',t,\lambda}}{d(r,r')}\right\|_2^2, \quad (19)$$

where V_r is the neighborhood of position r and $d(r,r')$ is the distance between position r and r'.

3.3.2 Edge preserving smoothness regularization

To avoid over-smoothing sharp features caused by quadratic regularization an edge preserving regularization can be used. This is achieved by replacing in Eq. (18) the quadratic norm by a norm φ that penalizes large difference less severely than quadratic norm:

$$\Omega_{\text{edge}}(\boldsymbol{x};t,\lambda) = \sum_r\varphi\left[(\mathbf{D}\cdot\boldsymbol{x}_{t,\lambda})_r\right], \quad (20)$$

In this work, we choose a ℓ_1–ℓ_2 norm. This norm is asymptotically quadratic (resp. linear) for small (resp. large) pixel value differences compared to a given threshold. It is defined by:

$$\varphi(u;\eta) = 2\eta^2\left[|u|/\eta - \log(1+|u|/\eta)\right]. \quad (21)$$

where the parameter η is a threshold selecting the level beyond which the difference between a pixel and one of his neighbor is due to an edge, and then must not be smoothed too much. The value of this parameter η is not critical for the reconstruction and can be approximately fixed to the value of one quantization level. In that case, this regularisation is close to a pure ℓ_1 regularization but can be minimized faster by our optimization algorithm.

With such a regularization function, the object spatial regularization $\Theta_{\text{obj}}(\boldsymbol{x};\boldsymbol{\beta^{\text{obj}}})$ defined in Eq. (19) can be rewritten as:

$$\Theta_{\text{obj}}(\boldsymbol{x};\boldsymbol{\beta^{\text{obj}}},\eta) = \sum_{t,\lambda}\beta^{\text{obj}}_{t,\lambda}\sum_r\sum_{r'\in V_r}\varphi\left(\frac{x_{r,t,\lambda}-x_{r',t,\lambda}}{d(r,r')};\eta\right). \quad (22)$$

3.3.3 Shape regularization

If the prior on $\boldsymbol{x}$ can be described by a parametric function $\boldsymbol{p}(\boldsymbol{\theta})$ of parameters $\boldsymbol{\theta}$, the deviation between $\boldsymbol{x}$ and this prior can then be taken as the regularization penalty [7]:

$$\Omega_{\text{shape}}(\boldsymbol{x};t,\lambda) = (\boldsymbol{x}_{t,\lambda} - \boldsymbol{p}(\boldsymbol{\theta}))^{\mathrm{T}} \mathbf{W}_{\text{shape}} (\boldsymbol{x}_{t,\lambda} - \boldsymbol{p}(\boldsymbol{\theta})), \qquad (23)$$

where $\mathbf{W}_{\text{shape}}$ is a weighting matrix. The function $\boldsymbol{p}(\boldsymbol{\theta})$, should have few parameters (width, direction of elongation...).

This regularization is well adapted to spatial regularization of the PSF. As there are many different causes of blur (defocus, motion, diffraction, diffusion...), there is a lot of totally different PSF shapes. In this context a parametric function $\boldsymbol{p}(\boldsymbol{\theta})$ (Gaussian, generalized Gaussian, Lorentzian...) can be chosen to set the prior shape of the PSF.

3.3.4 Spectral regularization for the object

In the case of a chromatic object $f_{r,\lambda}$, it is possible to let the spatial brightness distribution have a high dynamical range while constraining the spectral distribution to follow approximately the same law p_λ through the following regularization:

$$\Omega_{\Xi}(\boldsymbol{f};r,t) = \sum_{\lambda} \left[\frac{f_{r,t,\lambda+\Delta\lambda}}{p_{t,\lambda+\Delta\lambda}} - \frac{f_{r,t,\lambda}}{p_{t,\lambda}} \right]^2, \qquad (24)$$

where $p_{\lambda,t} = 1/N \sum_r f_{r,t,\lambda}$ is a charateristic synthetic spectrum (the mean spectrum in Sec. 5.2) at epoch t.

4. ALGORITHM SUMMARY

In our framework, the reconstruction of the the deblurred object corresponds to the determination of the couple $\{\boldsymbol{f}^+, \boldsymbol{h}^+\}$ that minimizes the criterion defined in Eq. (6), which writes:

$$\begin{aligned} \varepsilon =& \Phi_{\text{lkl}}(\boldsymbol{f},\boldsymbol{h};\boldsymbol{g}) \\ &+ \Psi_{\text{obj}}(\boldsymbol{f};\boldsymbol{\alpha}_{\mathbf{obj}}) + \Theta_{\text{obj}}(\boldsymbol{f};\boldsymbol{\beta}_{\mathbf{obj}}) + \Xi_{\text{obj}}(\boldsymbol{f};\boldsymbol{\mu}_{\mathbf{obj}}) \\ &+ \Psi_{\text{psf}}(\boldsymbol{h};\boldsymbol{\alpha}_{\mathbf{psf}}) + \Theta_{\text{psf}}(\boldsymbol{h};\boldsymbol{\beta}_{\mathbf{psf}}) + \Xi_{\text{psf}}(\boldsymbol{h};\boldsymbol{\mu}_{\mathbf{psf}}). \end{aligned} \qquad (25)$$

The optimal reconstructed image $\boldsymbol{f}^+$ and PSF $\boldsymbol{h}^+$ depend on the particular value of the hyper-parameters $\boldsymbol{\alpha}$, $\boldsymbol{\beta}$, and $\boldsymbol{\mu}$. Choosing the optimal values of the hyper-parameters is cumbersome and difficult. The large number of hyper-parameters defined in this very general scheme can be drasticly reduced according to simple rules as explained in Sec. 5.1.1. For the few (2 or 3) remaining tunable parameters, methods such as generalized cross-validation (GCV)[8] or the L-curve are suitable, but deserve an extensive study which is out of the scope of this paper. In the present work, we simply choose hyper-parameters values by visual inspection of the resulting image.

4.1 Minimization Method

In case of blind deconvolution, an alternate minimization scheme is used to minimize the criterion:

1. initialize the PSF its *a priori* shape $\boldsymbol{h}^{(0)} = \boldsymbol{p}(\boldsymbol{\theta})$,
2. estimate the optimal object $\boldsymbol{f}^{(k+1)}$ given the PSF $\boldsymbol{h}^{(k)}$,
3. estimate the optimal PSF $\boldsymbol{h}^{(k+1)}$ given the object $\boldsymbol{f}^{(k+1)}$,
4. repeat steps 2 and 3 until convergence or after a defined number (k) of iterations.

In order to determine the optimal image $\boldsymbol{f}^+$ and PSF $\boldsymbol{h}^+$ in our inverse problem approach, we have to minimize a criterion with respect to a very large number of variables (all the pixel values for every frames). To that end, we use the VMLM-B algorithm [9] which is a limited memory variant of the variable metric method with BFGS updates [10]. This algorithm, can further account for bound constraints on the parameters. We make use of this feature to enforce PSF positivity. This algorithm has proven its effectiveness for image reconstruction and only requires the computation of the penalty function being minimized and its gradient. The memory requirement is a few times the size of the problem.

5. RESULTS

5.1 Coronarography

The coronarography is a radiological exam to observe coronary arteries (heart arteries). This gives short (several seconds) video sequences displaying the motion of an impervious to X-ray product in the coronary arteries. These sequences are examined by a cardiologist to localize obstruction in the arteries caused by atherosclerosis, possibly responsible of an heart attack. Ten sequences were acquired and, as the blurring process is unknown, the (x,y,t) object is reconstructed using the blind deconvolution scheme. Every sequences were acquired with the same system and were processed under the same assumptions.

5.1.1 Regularization and hyper parameters settings

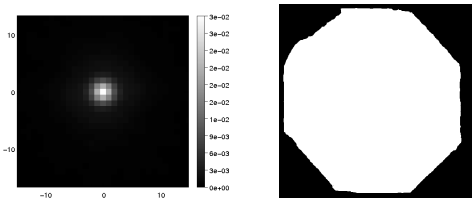

(a) Estimated PSF (30 × 30)

(b) Weight map (512× 512)

Figure 1: Estimated PSF and weight map used for coronarography sequence shown in Fig. 2

Several specificities can be noticed by a simple observation of the raw data (see Fig. 2(a)) and can be used to define regularization functions and hyper-parameters for both the object and the PSF:

(i) A shape constraining regularization as defined in Eq. (23) with a Lorentzian prior shape $p(\theta)$ appears to be a good prior; hence $\Theta_{\text{psf}}(\boldsymbol{x};\boldsymbol{\beta}_{\mathbf{psf}}) = \Omega_{\text{shape}}(\boldsymbol{x})$. The parameter θ is then the full width at half maximum of the Lorentzian.

(ii) As the blur seems to be caused by tissue in the axis of projection, and as neither the patient nor the acquisition system was moving during the recording, the PSF is supposed to be constant. As a consequence, $\boldsymbol{h}_{r,t} = \boldsymbol{h}_r$, $\forall t$. In that case the number of unknown parameters on the PSF is divided by T, increasing the computation speed and robustness.

(iii) The frames contain sharp objects (coronaries) on a smooth background. We therefor use a edge preserving spatial regularization as defined in Eq. (22): $\Theta_{\text{obj}}(\boldsymbol{x};\boldsymbol{\beta}_{\mathbf{obj}},\boldsymbol{\eta}) = \Omega_{\text{edge}}(\boldsymbol{x},\boldsymbol{\eta})$. Image dynamic is constant in every frames.

As a consequence, both the object and PSF spatial hyper-parameters and object threshold are constant for each frame:

$$\beta_t^{\text{psf}} = \beta_{\text{psf}},\ \beta_t^{\text{obj}} = \beta_{\text{obj}}, \text{ and } \eta_t = \eta,\ \forall t. \tag{26}$$

(iv) The motion of the heart is too important between successive frames to make use of a temporal continuity on the object. So we didn't use temporal regularization on the object, thus $\Psi_{\text{obj}}(\boldsymbol{x}) = 0$.

(vi) The noise is assumed to be Gaussian and uncorrelated and we use the likelihood penalty defined in Eq. (10).

(vii) The measured area is not square and is cropped by some parts of the apparatus which remains the same in every frame of every sequence. This is taken into account by simple thresholding and by defining the weight map used in Eq. (10) as:

$$w_{r,t} = \begin{cases} 1 & \text{if } k\text{-th pixel is above threshold,} \\ 0 & \text{otherwise.} \end{cases}, \tag{27}$$

and which is shown in Fig. 1(b). Finally only three hyper-parameters have to be determined to perform this blind deconvolution: $\beta_{\text{psf}}, \beta_{\text{obj}}$ and θ.

5.1.2 Results

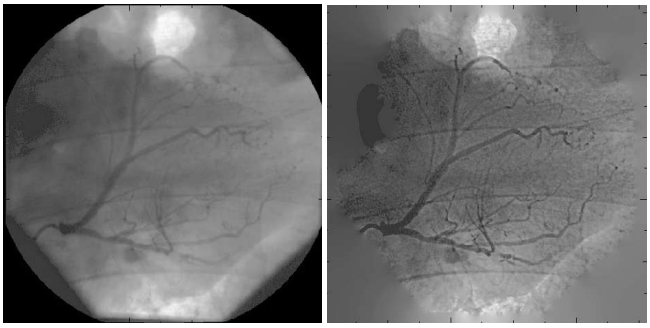

(a) Raw image (b) Reconstruction of 2(a)

Figure 2: One frame of a coronarography sequence

10 sequences of about 75 frames of 512×512 pixels were processed in about 80 seconds per frame. The assumption of an identical PSF in every frames of a same sequence considerably constrains the PSF and leads to a robust estimation of $\boldsymbol{h}^+$. We also tried relaxing this temporal constraint on the PSF, but it did not show significant improvements, which confirms the validity of our assumption of a constant PSF. A frame out of the studied sequences is shown in Fig. 2(a), along with the corresponding restored frame, the estimated PSF is shown in Fig. 1(a). Although the working quantization interval was very small (at most 10 digital levels between pixels in the arteries and the background), a visual assessment shows the effectiveness of our technique (especially, for micro-arteries reconstruction). Motion perception in the deconvolved video sequences is greatly improved as the separation of the coronaries and the background is enhanced. We point out that the cropped area does not impact the deconvolution, even for pixels close to the border of this area. These unmeasured parts are simply filled with uninformative smooth background in accordance with the smoothing prior. These restored sequences were shown to cardiologists who confirmed the potential utility of the presented technique. If this method proves efficiency with noisier sequences, cardiologists can consider a decrease of the X-ray beam to reduce irradiation of patients and physicians.

5.2 Integral Field Spectrography

The SuperNova factory is a survey using an integral field spectrograph to observe type Ia supernovae (SNeIa) in the redshift range $0.03 < z < 0.08$ [11]. The observed supernovae are point source objects on top of the structured background of their host galaxy. A PSF can be extracted from photometric exposures taken simultaneously to the spectroscopic exposures.

To assess the performance of our algorithm on (x, y, λ) images cubes, we process simulation made for the SuperNova factory survey. These simulations include realistic PSF and noise. They produce (15×15) pixels images at 798 different wavelengths from 3200Å to 5097Å. In this work we achieve reconstruction of the (x, y, λ) data cube using the extracted PSF, by a multi-wavelength regularized deconvolution.

5.2.1 Regularization and hyper parameters settings

As in the coronarography example, observations of the raw data (see Fig. 3(a)) can be used to defined regularization functions and hyper-parameters on the object:

(i) The frames contain a smooth and cropped galaxy contaminated by strong noise. We use the spatial regularization function defined in Eq. (19). Due to strong spectral features (mostly absorption lines and bands), the light flux is highly variable at the different wavelengths. As a consequence, the object spatial hyper-parameters have to be different for each frame. That is why we propose a normalization of these hyper-parameters by the variance $\text{Var}(g)_\lambda$ in each frames λ:

$$\beta_\lambda^{\text{obj}} = \frac{\beta_{\text{obj}}}{\text{Var}(g)_\lambda}, \forall \lambda, \tag{28}$$

hence β_{obj} is the only spatial hyper-parameter to be tuned instead of 798.

(ii) Our prior is that the spectrum of each pixel approximately follows the same law p_λ and we use the regularization defined in Eq. (24) with a single hyper-parameter: $\mu_r^{\text{obj}} = \mu_{\text{obj}},\ \forall r$.

(iii)As the noise is Poissonian and uncorrelated, we use the likelihood penalty defined in Eq. (10) with weight defined as in Eq. (12).

(iv) As the PSF is almost as wide as the field of view, the working area is extended to (32×32) pixels per frame. The weights in Eq. (10) of the unmeasured pixels are set to 0. This extension of the working area is necessary to rigorously cope with the extent of the PSF, and allows some level of field of view extrapolation.

Finally only two hyper-parameters have to be determined to perform this deconvolution: $\beta_{\text{obj}}, \mu_{\text{obj}}$.

5.2.2 Results

The data processed by our algorithm was simulated with only the host galaxy at the Supernova minimum. Image taken at $\lambda = 3968$Å, its reconstruction and corresponding ground truth are shown on Fig. 3. On this figure the reconstruction and the ground truth are truncated to the field of view of the sensor. A

visual assessment shows the effectiveness of our technique. Although a strong noise is present in the data, the reconstruction presents details that were not visible in the data. For example the bright center of the galaxy which is difficult localize in the raw data is well resolved in the reconstruction. The reconstructed spectrum (dashed red) of the central pixel is shown on Fig. 3(e) with corresponding spectrum of data (blue dotted) and ground truth (black line).

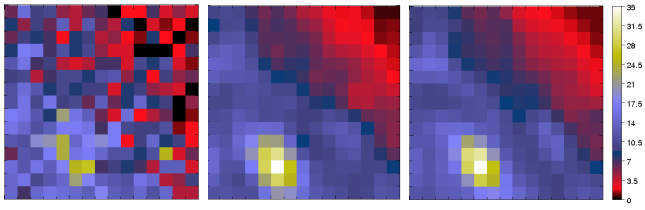

(a) Raw image (b) Reconstruction (c) True image

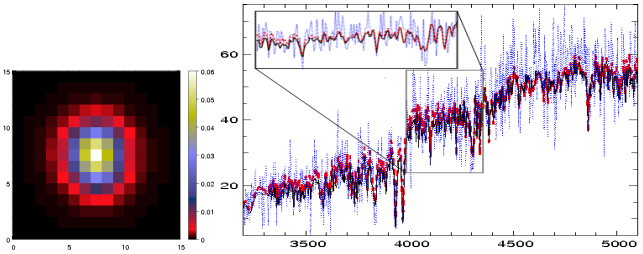

(d) PSF at $\lambda = 3968.74$Å (e) Spectrum of the central pixel.

Figure 3: Images (15×15) and PSF at $\lambda = 3968.74$Å

To quantify the reconstruction quality, we use the *Peak Signal to Noise Ratio* (PSNR) which is classically used to measure improvements of digital image quality. This criterion corresponds to a mean squared error normalized by the maximum pixel value M:

$$E_{\mathrm{PSNR}}(\hat{\boldsymbol{x}}) = -10 \log_{10}\left(K^{-1} M^{-2} \sum_{\lambda,r} \left(\hat{x}_{\lambda,r} - f^{\mathrm{true}}_{\lambda,r}\right)^2 \right), \quad (29)$$

where $K = N \cdot L$ is the number of pixels, $\hat{\boldsymbol{x}}$ and $\boldsymbol{x}$ are respectively the restored and the true images. Thus, the larger is the PSNR, the better is the reconstruction. We measured the data distortion $E_{\mathrm{PSNR}}(\boldsymbol{g}) = 25.9$dB and the reconstruction ones (cropped to the data size) $E_{\mathrm{PSNR}}(\boldsymbol{f}+) = 36.2$dB.

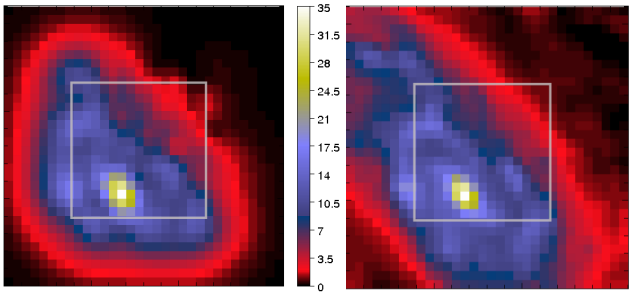

(a) Reconstruction of 3(a) (b) True image

Figure 4: Image (32×32) at $\lambda = 3967$Å with extrapolation

If we compare the true image to the reconstruction outside of the field of view on Fig. 4 (outside of the grey square), we see that the extrapolation is not uninformative. The general inclined shape of the galaxy is reconstructed and more, the position of its spiral harms can be guessed on the reconstruction (especially on the top left corner). If we consider the extrapolation, the measured PSNR of the reconstruction is $E_{\mathrm{PSNR}}(\boldsymbol{f}) = 33.6$dB.

This (x, y, λ) data cube was processed by our algorithm in several hours. This relative slowness can be explained by the bad conditioning of the optimization process, as it must determine the value of (32×32) pixels per frames using (15×15) measurements per frame (4 unknown for 1 data) and propagate information far from the field of view.

6. CONCLUSION

In this paper, we present a new algorithm for deconvolving heterogeneous multidimensional data. We show results on two very different data sets. For each we explain the choice of regularizations according to the data formation. These results show the strength of separable regularizations for each dimension for enhancing the the effectiveness and the robustness of both blind and non-blind deconvolution process compared to independent deblurring of successive images.

REFERENCES

[1] P. Campizi and K. Egiazarian, Eds., *blind image deconvolution: theory and application*, CRC Press, 2007.

[2] T. J. Schulz, "Multiframe blind deconvolution of astronomical images," *J. Opt. Soc. Am. A*, vol. 10, no. 5, pp. 1064–1073, may 1993.

[3] D. Li *et al.* "New method for suppressing optical turbulence in video," in *Proc. EUSIPCO*, 2005.

[4] J.A. Aguilera *et al.* "Spatial characterization of laser-induced plasmas by deconvolution of spatially resolved spectra," *Appl. Opt*, vol. 42, no. 30, pp. 5938–5946, 2003.

[5] F. Courbin *et al.* "A Method for Spatial Deconvolution of Spectra," *The Astrophysical Journal*, vol. 529, pp. 1136–1144, Feb. 2000.

[6] E. Thiébaut and J.-M. Conan, "Strict a priori constraints for maximum likelihood blind deconvolution," *J. Opt. Soc. Am. A*, vol. 12, no. 3, pp. 485–492, March 1995.

[7] A. Tarantola, *Inverse Problem Theory - Methods for Data Fitting and Model Parameter Estimation*, Elsevier, 1987.

[8] Gene H. Golub *et al.* "Generalized cross-validation as a method for choosing a good ridge parameter," *Technometrics*, vol. 21, pp. 215–223, 1979.

[9] E. Thiébaut, "Optimization issues in blind deconvolution algorithms," in *Astronomical Data Analysis II* SPIE, 2002, vol. 4847, pp. 174–183.

[10] Jorge Nocedal, "Theory of algorithms for unconstrained optimization," *Acta Numerica*, vol. 1, pp. 199–242, 1992.

[11] G. Aldering *et al.* "Overview of the Nearby Supernova Factory," in *Survey and Other Telescope Technologies and Discoveries*, J. A. Tyson and S. Wolff, Eds., Dec. 2002, vol. 4836 of *(SPIE) Conference*, pp. 61–72.